Available online at www.sciencedirect.com

jmr&t Journal of Materials Research and Technology

journal homepage: www.elsevier.com/locate/jmrt

Original Article

Dynamic compression of a polymer stamper using high-impulse underwater shock waves to imprint a sub-micrometer structure on a metal plate surface

Kouki Hasegawa [a], *Shigeru Tanaka* [b,*], *Daisuke Inao* [c], *Masatoshi Nishi* [d], *Akihisa Kubota* [a], *Kazuyuki Hokamoto* [b]

[a] *Graduate School of Science and Technology, Kumamoto University, 2-39-1 Kurokami, Chuo-ku, Kumamoto-shi, Kumamoto 860-8555, Japan*

[b] *Institute of Industrial Nanomaterials (IINa), Kumamoto University, 2-39-1 Kurokami, Chuo-ku, Kumamoto-shi, Kumamoto 860-8555, Japan*

[c] *Technical Division, Faculty of Engineering, Kumamoto University, 2-39-1 Kurokami, Chuo-ku, Kumamoto-shi, Kumamoto 860-8555, Japan*

[d] *National Institute of Technology, Kumamoto College, 2627 Hirayama-Shinmachi, Yatsushiro-shi, Kumamoto, 866-8501, Japan*

ARTICLE INFO

Article history:
Received 16 March 2023
Accepted 27 April 2023
Available online 2 May 2023

Keywords:
Nanoimprint lithography
Laser shock imprinting
Meta-surface
Explosive materials processing
Autodyn

ABSTRACT

Press-forming technology is excellent for mass production. However, for micrometer-order forming, manufacturing press tools is unprofitable. Because laser-induced shock waves cannot rapidly accelerate heavier workpieces into molds, the workpieces are limited to thin metal foils. In this study, an explosion-derived high-impulse shock wave was applied to dynamically compress a polymer stamper into a metal plate. The stamper was pressed for a few microseconds, resulting in a well-imprinted submicron structure on the aluminum plate surface. Numerical simulation clarified the imprinting mechanism, which involved local compression and restoration of the stamper profile that occurred when the reflected shock wave generated at the boundary between the stamper and the workpiece reached the free surface of the stamper. It was discovered that the shock wave must continue to act for a significantly longer time than that required for the reflected shock wave to reach the free surface of the stamper. Therefore, explosion-derived shock waves with a long pressure duration are effective for imprinting. This method has the potential to be developed into a practical technique for imparting functional microsurfaces to structural components.

* Corresponding author.
E-mail addresses: hasegawa@mech.kumamoto-u.ac.jp (K. Hasegawa), tanaka@mech.kumamoto-u.ac.jp (S. Tanaka), inao@tech.kumamoto-u.ac.jp (D. Inao), nishima@kumamoto-nct.ac.jp (M. Nishi), kubota@mech.kumamoto-u.ac.jp (A. Kubota), hokamoto@mech.kumamoto-u.ac.jp (K. Hokamoto).

https://doi.org/10.1016/j.jmrt.2023.04.248

1. Introduction

Recently developed laser shock imprinting (LSI) [1,2] uses laser-induced shock waves and high-quality silicon or nickel electroformed nanomaterials prepared using nanoimprint lithography [3] or electron beam lithography [4] to imprint on metallic foil surfaces in the range of nanometers. In this technique, a thin metallic foil is compressed into a hard mold. The mechanism for forming a workpiece true to the mold is related to the plastic flow of the workpiece associated with the emergence of a high strain rate field exceeding 10^6–10^7/s [5,6]. The mold, which exhibits no deformation during the shock compression process, is the source of the high strain field [1,7]. Although LSI, which is used for fabricating metallic nanostructures in a single step, is more efficient than other lithographic techniques (that are multi-step and time-consuming processes), it requires expensive nanomolds, which are damaged during shock compression [8–10]. This is a significant disadvantage of LSI.

Recent studies on LSI have focused on incorporating the use of inexpensive polymer molds. Copying a nanomold with a photo or thermosetting polymer is relatively easy [11]. Goswami et al. used titanium particle composite epoxy nanomolds to achieve nanoimprinting on a metal that was deposited on a polyethylene terephthalate film [12]. Imprinting can also be achieved on freestanding metal workpieces, such as metal foils. Jin et al. replicated the microstructures of a bamboo leaf surface using an ultraviolet-curable polymer as a mold for LSI, and they successfully imprinted an aluminum (Al) foil with the leaf microstructure. The recovered metallic leaves had a strong water-repellent property, similar to that of the bamboo leaves, and demonstrated frictional power generation by the rolling of raindrops [13]. Furthermore, they focused on the submicron-order periodic sinusoidal surface structure of an optical disc (DVD). The DVD was composed of polycarbonate (PC). The PC was used as a mold, and the obtained samples acquired surface plasmon resonance [14]. These studies demonstrated that functional surfaces can be produced using polymer molds.

The processing area of LSI is limited to the laser irradiation range. Therefore, achieving imprinting beyond an area of 1 cm^2 through a single shot is difficult. To achieve large-scale imprinting, recent studies have focused on shock imprinting using explosion-derived shock waves. High imprinting accuracy and large-area imprinting have been demonstrated using underwater shock waves derived from explosions exerting a high pressure over a wide area [15–17].

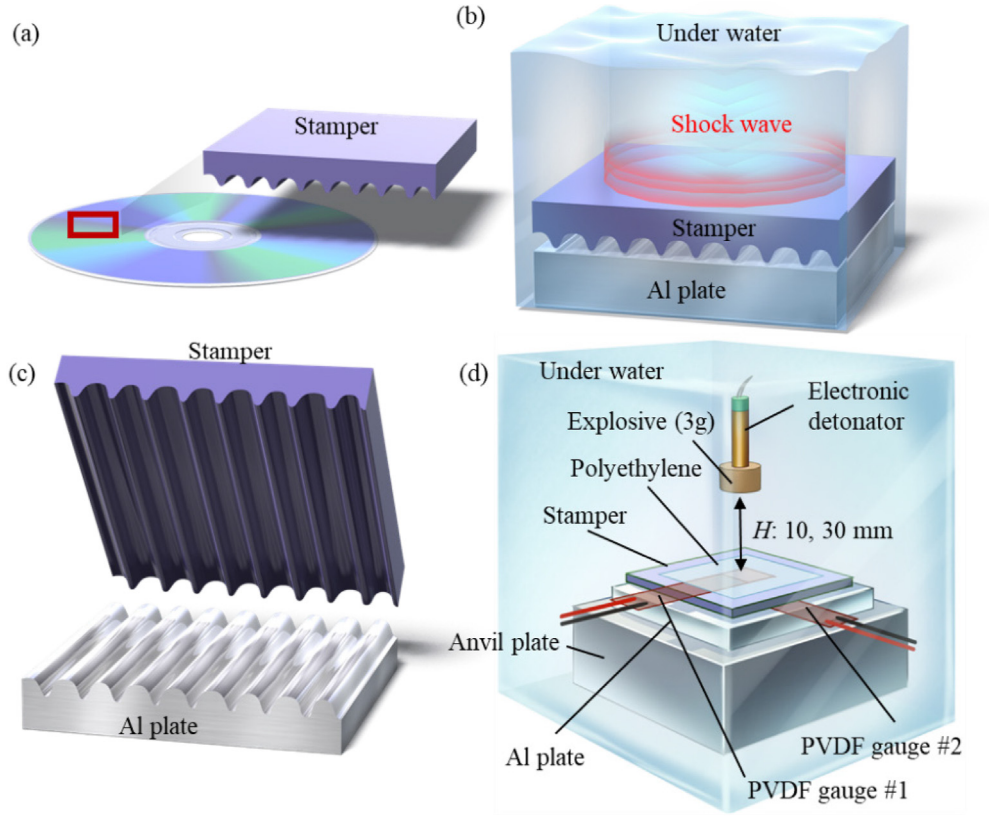

Fig. 1 – Schematic of the impact imprint process and pressure measurement experiment using a polymer stamper. (a) Preparation of the DVD stamper. (b) Stamper and Al workpiece subjected to the underwater shock wave. (c) Imprinted Al workpiece. (d) Layout of the pressure measurement experiment.

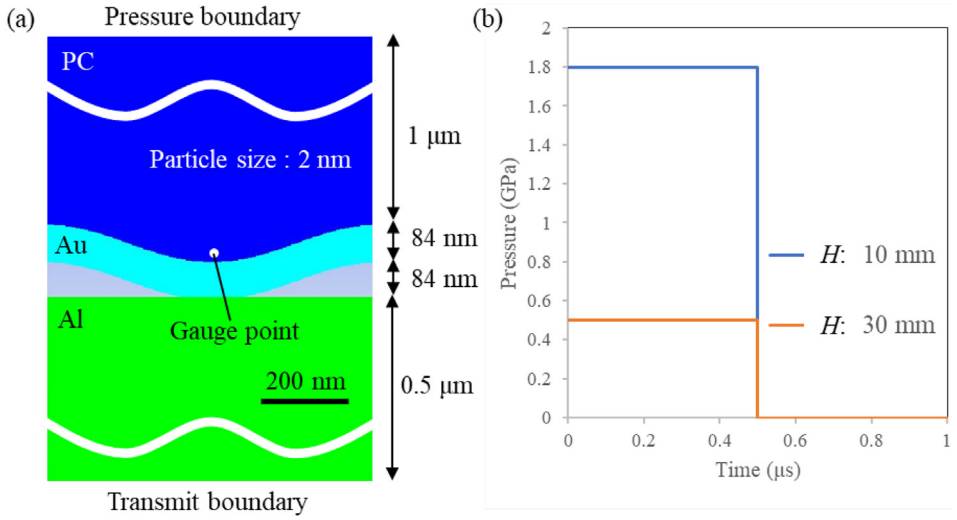

Fig. 2 – The simulation model and initial conditions. (a) 2D SPH model. (b) Initial pressure conditions.

Jin et al. conducted a numerical analysis of the dynamic deformation between the metal workpiece and polymer mold and found that the mechanism of shock imprinting using the polymer molds is based on the fact that the sound velocity in the polymer is lower than that in the metal workpiece [13] (i.e., the metal workpiece deforms faster than the polymer mold). Therefore, in previous studies, thin workpieces were used to reduce the polymer mold deformation [13–17]. Thin foils were used even for micro- and nano-scale imprinting studies using hard molds [1,2,7,18–21].

Hasegawa et al. conducted sub-millimeter-order shock-forming experiments and numerical simulations to investigate the dynamic interaction between the polymer mold and the metal workpieces. They found that the polymer mold deformed easily during processes with pressures in order of several hundred MPa to several GPa. The original mold shape recovered during the pressure relaxation process, and this recovery strongly affected the final shape of the workpiece [22]. If the metal workpiece deforms during the end of the process, the thin metal foil is not required. Imprinting can be achieved by pressing the polymer mold onto the metal plate material. Currently, shock-imprinting techniques have been limited to foil materials being used as the processing targets. Using plate materials as the processing targets may result in structural components with functional properties.

The objectives of this study are as follows: First, we demonstrate the technique for microimprinting metal plates using a polymer stamper. The second objective is to understand the imprinting mechanism of this new technology. In this study, a submicron-order sinusoidal structure on the surface of a DVD was used as the stamper. Explosives were used as the source for shock waves to achieve large-area imprinting. Submicron-scale numerical simulations were performed to investigate the dynamic deformation process and to describe the micro-scale multi-physics behavior at the interface between the reflected shockwave and the stamper. This study proposes an unconventional imprinting concept that uses a polymer stamper, which is softer than the metal workpieces.

2. Experimental and numerical simulation

2.1. *Stamping on metal with polymer*

In previous shock-imprinting studies, a thin metal foil was compressed into a mold. In contrast, in this study, a polymer mold was compressed onto a metal plate. This method involves simple stamping. The only novel step is the explosion that creates the shockwave. The process of this method, along with the layout of the explosives and samples (stamper and the metal plate) are shown in Fig. 1. The DVD (DHR47JDP Verbatim Japan, Tokyo, Japan) without the protective plate was cut into several 30 mm squares, and the stamper was prepared (Fig. 1 (a)). A PC stamper was used, and a reflective silver film was deposited on its surface. The stamper thickness was 0.8 mm. The sinusoidal structure of the surface had a period of 740 nm and wave height of 84 nm (details of the stamper geometry are given in Section 3). The DVD was used because it is inexpensive, and its surface topography shows excellent uniformity. This makes it suitable as a stamper for laboratory-level experiments. The stamper was overlaid on an Al plate. They were packed inside a polyethylene bag for waterproofing and decompressed to an internal pressure of 0.01 MPa. Subsequently, they were placed under water. For the shock wave source, 3.0 g of a pentaerythritol tetranitrate (PETN)-based explosive (SEP, 6970 m/s, 1310 kg/m^3, Kayaku Japan Co., Ltd., Tokyo, Japan) was used. PETN is a powdered explosive with a density of 1770 kg/m^3 and a detonation heat of 5.81 kJ/g [23]. A cylinder-shaped explosive with a diameter of 18 mm was used, and it was detonated underwater using an electric detonator at a distance H from the stamper. Water was used as the medium because it could transmit the pressure while blocking the detonation heat. The underwater shock wave generated by the explosion acted on the stamper (Fig. 1 (b)), imprinting the stamper microstructure on the Al plate surface (Fig. 1 (c)). The Al plate was A1050-O with a thickness of 5.0 mm. The stamper and imprint geometries

were evaluated using atomic force microscopy (AFM) (SPM-9700, Shimadzu Co., Ltd., Kyoto, Japan).

In this study, the pressure of the underwater shock wave was the only variable. The shockwave pressure attenuates as H increases. The pressure value of the shock wave acting on the stamper is necessary for numerical simulations. The layout of the pressure measurement experiment is shown in Fig. 1(d), which is the same as that of the imprint experiment. Piezoelectric film gauges (PVDF) (PVF2-11-0.125-EK, Dynasen Inc., Goleta, CA, USA) were glued onto the PC stamper (#1) and Al plate (#2). The film gauge was connected to an oscilloscope (DPO7254C, Tektronix Inc., Beaverton, OR, USA) through a charge integrator (CI-50-0.1, Dynasen Inc., Goleta, CA, USA). The pressure measurements were performed at values of H: 10 and 30 mm.

2.2. Numerical simulation

ANSYS Autodyn 19.2 software was used for the numerical analysis. The model assumed a plane strain field, and a 2D smooth particle hydrodynamics (SPH) solver was used. The model diagram is shown in Fig. 2 (a). AFM was used to measure the geometry of the stamper (period: 740 nm, height: 84 nm). The stamper was composed of a PC and a reflective deposition film, gold (Au), which is similar to that used in the study conducted by Jin et al. [14]. PC possesses a significant strain-rate hardening effect [24]. The thickness of the deposition film was set to 84 nm, which is the same as the amplitude of the PC sine wave [25]. The Al plate was modelled below the stamper. To reduce the computation time, the thicknesses of the PC and Al plates were set to 1 and 0.5 μm, respectively. The stepped pressure, as shown in Fig. 2 (b), was used as the initial condition on the top surface of the PC that was set up as a stamper, based on the peak pressure measured in the pressure measurement experiment under the $H = 30$ mm condition. This analysis assumes that the shock waveform is constant because it terminates after a few nanoseconds, which is sufficiently shorter than the duration of the shock wave action. All particles in this analysis were discretized to a size of 2 nm.

The material boundaries were assumed continuous, and the movement was restricted to the longitudinal direction. A1100-O, PC, and Au material properties were used in this model. These materials were modelled using the Mie–Gruneisen equation of state (EOS) based on the Hugoniot data as follows:

$$p = p_H + \Gamma\rho(e - e_H), \tag{1}$$

$$\Gamma\rho = \Gamma_0\rho_0 = \text{const}, \tag{2}$$

$$p_H = \frac{\rho_0 c_0^2 \mu(1+\mu)}{(1-(s-1)\mu)^2}, \tag{3}$$

$$e_H = \frac{1}{2}\frac{\rho_H}{\rho_0}\left(\frac{\mu}{1+\mu}\right), \tag{4}$$

where p is the pressure, P_H is the Hugoniot pressure, Γ is the Gruneisen gamma, ρ is the density, e is the internal energy, e_H is the Hugoniot internal energy, Γ_ρ is the Gruneisen gamma of the reference state, ρ_0 is the initial density, c_0 is the bulk velocity of the sound, μ is the compression, and s is the linear Hugoniot gradient coefficient. Table 1 lists the parameters of the Mie–Gruneisen EOS for A1100-O, PC, and Au.

An accurate characterization of the mechanical properties of the materials subjected to high strain rate deformation is very complex because of the simultaneous effects of several phenomena, such as workpiece hardening, strain rate hardening, and thermal softening. In this case, the yield stresses of A1100-O, PC, and Au were estimated using the Johnson–Cook elasto-viscoplastic material model [29]. The equivalent von Mises yield stress (σ_y) is defined as follows:

$$\sigma_y = \left(A + B\varepsilon_p^n\right)\left(1 + C\ln\dot{\varepsilon}_p^*\right)(1 - T^{*m}), \tag{5}$$

where A, B, n, C, and m are the material parameters, ε_p is the equivalent plastic strain, $\dot{\varepsilon}_p^* = \dot{\varepsilon}/\dot{\varepsilon_{ref}}$ is the dimensionless strain rate, and T* is the dimensionless temperature. The dimensionless temperature is defined as $\{T^* = (T - T_{room})/(T_m - T_{room})\}$. Additionally, $\dot{\varepsilon}$ is the strain rate, $\dot{\varepsilon_{ref}}$ is the reference strain rate, T is the current temperature, T_m is the melting temperature of the alloy, and T_{room} is the room temperature.

Since the imprint phenomenon may be closely related to material failure, the Johnson–Cook fracture model [29] was used in the numerical analysis to analyze the behavior of the A1100-O under high-strain conditions. In this model, the equivalent strain to fracture ε_f is defined as follows:

$$\varepsilon_f = \left(D_1 + D_2 e^{D_3\sigma^*}\right)\left(1 + D_4\ln\dot{\varepsilon}_p^*\right)(1 + D_5 T^*), \tag{6}$$

where D_1–D_5 are the material parameters, $\sigma^* = \sigma_m/\sigma_{eq}$ is the stress triaxial ratio, σ_m is the mean stress, and σ_{eq} is the equivalent von Mises stress. Depending on the equivalent fracture strain, the damage parameters were calculated as follows:

$$D = \Sigma\frac{\Delta\varepsilon}{\varepsilon_f}. \tag{7}$$

Here, D is the damage parameter, which is assumed to be equal to one when the material is destroyed and <1 when intact, and $\Delta\varepsilon$ is the change in plastic strain. Table 2 lists the parameters of the Johnson–Cook constitutive and fracture laws for A1100-O, PC, and Au used in this analysis.

3. Results and discussion

3.1. Imprint experimental results

The details of the samples recovered in the imprint experiment are shown in Fig. 3. Fig. 3 (a) is a picture of the

Table 1 – Mie-Gruneisen EOS parameters for A1100-O [26], PC [27], and Au [28].

	A1100-O	PC	Au
Reference density (kg/m^3)	2.707	1.197	19.24
Gruneisen gamma	1.970	0.61	2.97
c_0 (m/s)	5386	1933	3056
s	1.339	2.6050	1.572
Reference temperature (K)	293	293	293

Table 2 – Jonson–Cook strength and failure model parameters for A1100-O [30,31], PC [14], and Au [14].

	A1100-O	PC	Au
A (MPa)	49	75.8	120
B (MPa)	157	68.9	243
C	0.016	0.052	0.056
n	0.167	1	0.147
m	1.7	1.85	0
D_1	0.071	–	–
D_2	1.248	–	–
D_3	−1.142	–	–
D_4	0.0097	–	–
D_5	0.0	–	–

appearance of a sample recovered under the condition of $H = 30$ mm. A 30 × 30 mm^2 area of a 5 mm thick Al plate showed a clear structural color. Fig. 3 (b) and (c) presents the surface profiles and 3D images, respectively, of the stamper and Al plates recovered under each condition, as measured using AFM. The stamper originally had a sinusoidal structure with a wave height and period of 84 and 740 nm, respectively. In the experiment, the smaller the height H, the higher the pressure acting on the stamper. For $H = 10$ mm, the average value of the imprinted wave height was 41 nm despite the high-pressure condition. The 3D image also shows a rough surface texture. The average imprint wave height was 58 nm for $H = 30$ mm. The maximum peak-wave height was 64 nm. Therefore, an imprint wave height of approximately 69% of that of the stamper was formed. The 3D images show smooth surface properties. In an LSI study by Jin et al. using a DVD mold, grooves with a depth of 40 nm were formed on an Al foil with a thickness of 4 μm. In our study, the imprints on the plate material were deeper than that achieved the foil material, which is a significant milestone. The expansion of the pressure working area can be easily achieved by changing the shape of the explosive [32]. Using an explosive allows for imprinting over a larger area.

3.2. *Pressure measurement result*

The results of the pressure measurement experiment corresponding to the distance H are shown in Fig. 4. Fig. 4 (a) shows the results for $H = 10$ mm and the pressure history with the time of detonation for the electric detonator as 0 ns. The gauge #1 glued to the stamper outputs a characteristic profile that rises during the imprinting step. The PVDF gauge manufacturer recommends that the gauge be glued to a rigid body [33]. In this experiment, gauge #1 was glued onto a non-rigid PC, which absorbed the shock pressure. Therefore, a plateau pressure (step) is observed for gauge #1. The reflected shock-wave generated at the boundary between the stamper and workpiece propagated through the PC and travelled to the free surface of the stamper. When it reached the free surface, gauge #1 output the peak pressure. The rapidly rising output of gauge #2 indicates that the shock wave propagated in the PC arrived at gauge #2, which promptly output a peak pressure. Fig. 4 (b) presents the pressure history for $H = 30$ mm. The formation of the profiles for gauges #1 and #2 are similar to that in the case of $H = 10$ mm. Compared with the results corresponding to $H = 10$ mm, the pressure values show a clear pressure decay with an increasing H. A notable feature of both the results is the length of the pressure duration. The underwater detonation of explosives produces a high-impulse shock wave. The initial pressure values applied to the numerical simulation were the plateau pressure wave outputs of

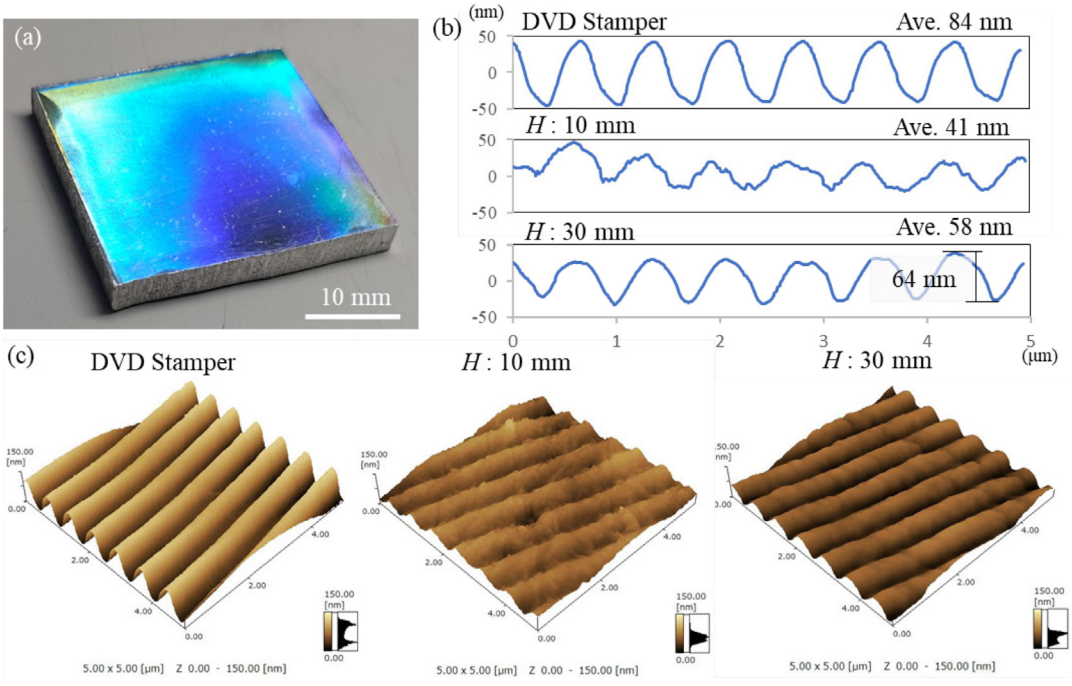

Fig. 3 – Recovered Al plates and original DVD stamper evaluated by AFM. (a) Sample appearance (H: 30 mm). (b) Surface profiles of stamper and imprinted specimens. (c) 3D surface of stamper and imprinted specimens.

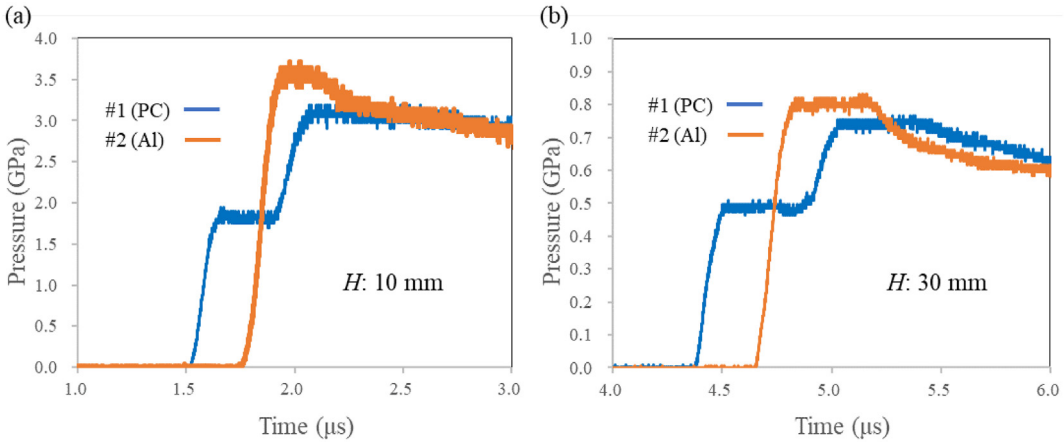

Fig. 4 – Pressure history corresponding to the distance *H* from the explosive to the sample. (a) 10 mm. (b) 30 mm.

gauge #1 from the pressure measurements and were equal to 1.8 and 0.5 GPa for $H = 10$ mm and 30 mm, respectively.

3.3. *Numerical simulation results*

Good imprinting was achieved for $H = 30$ mm. The numerical simulation results for a constant pressure input (0.5 GPa) are shown in Fig. 5. The left and right sides of the simulation images at the characteristic times show the deformation and internal pressure distributions of each element, respectively. The gauge point in the 0.00 ns image is the gauge point of the physical quantities in the simulation. The timestamp in each image shows the elapsed time, with 0 ns being the time immediately before the incident shock wave approaches the gauge point. The shock waves propagating inside the PC were reflected at the boundary of the Au deposition layer and gathered above the stamper convexity. Consequently, a local high-pressure field appeared in the PC (the area enclosed by the red dashed line at 0.08 ns). The height of the sinusoidal wave decreased when the stamper was compressed into the Al. Note that there was a pronounced deformation on the Al side (0.50 ns). A numerical analysis by Jin et al. demonstrated that the metal deposition layer contributes to the maintenance of the sinusoidal structure of the PC [14]. Our study also obtained similar results. When the stamper is fully compressed into the Al, the sinusoidal wave height decreases to 42 nm (0.66 ns). The sinusoidal wave height then begins to recover. This phenomenon began from 0.80 ns owing to the appearance of a local low-pressure field created on the surface of the PC, as shown in the area enclosed by the white dashed line. The sine wave height eventually recovers to 67 nm (1.68 ns).

The history of the changes in the pressure and specific volume of the gauge point is shown in Fig. 5 (b). The changes in the physical quantities before and after the shock wave followed the Rankine–Hugoniot equation [28]. Therefore, the pressure and specific volume of the PC are inversely related. The pressure change, despite the initial condition of 0.5 GPa, immediately increases to 1.2 GPa due to the convergence of the reflected shock wave generated at the boundary between the PC and Au. Section #1 shows the pressure release in the subsequent history, which indicates that the deformation of the stamper and Al spread into the free space. The increase in the pressure in section #2 can be attributed to the free space being filled with the deformation. The drop in the section #3 pressure was caused by the reflected shock waves generated at each boundary reaching the free surface of the PC. At this point, the specific volume began to increase. In the time that followed, the specific volume of the PC began to decrease, but the deformation of the Al had already reached the plastic region. During the simulation, the stamper continued to be compressed into the workpiece because the pressure at the gauge point was always positive. The shape-restoring force of the stamper surface caused by the reflected wave is one of the important factors in achieving a good imprint.

In the numerical simulation corresponding to $H = 10$ mm, a pressure of 1.8 GPa was exerted. The simulation images for the characteristic timings are shown in Fig. 6. The stamper was fully compressed into the Al, as shown in the image, at 0.52 ns. The high pressure reduces the shape-retention efficacy of the metal deposition layer. Consequently, the sinusoidal wave height was temporarily reduced to 29 nm. The sinusoidal wave height eventually recovered to 57 nm (1.52 ns). This value is smaller than the corresponding result of the analysis for $H = 30$ mm. The deformation mechanism was the same as that for $H = 30$ mm. This result implies the existence of ideal pressure conditions that lead to the achievement of a good imprint.

The shape recovery of the PC owing to the sudden pressure drop is caused by the reflected shock wave reaching the free surface of the PC, as described previously. Additionally, the Al continues to be compressed by the underwater shock wave during the shape recovery of the PC. The actual PC thickness of 0.8 mm was modelled in the simulation as 1 μm. Assuming that the speed of sound corresponding to the PC was 2000 m/s, the actual time required for the reflected shock wave to reach the free surface of the stamper was 400 ns. Notably, a significant difference exists between the simulation and actual phenomenon in terms of the time at which the shape restoration of the stamper occurs. However, as shown in Fig. 4, a characteristic property of the explosive-derived shock waves is their long duration of action (in the order of microseconds). This is compensated for by noting that the compression caused by the underwater shock wave continues to act for a

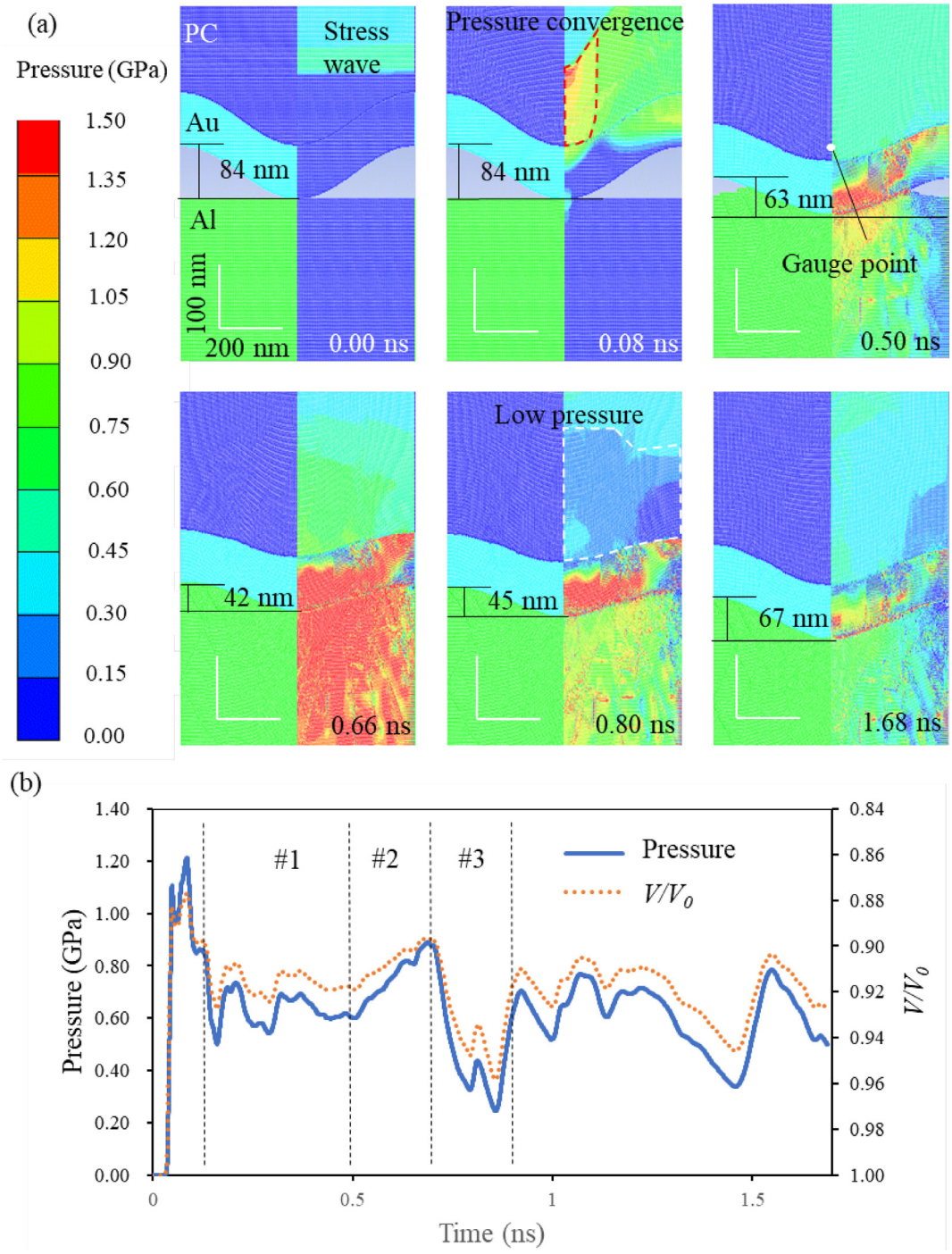

Fig. 5 – Dynamic deformation process of the stamper and Al workpiece reproduced via numerical simulation and changes in the internal pressure distribution ($H = 30$ mm). (a) Deformation and internal pressure distribution. (b) Pressure and specific volume change in PC convexity.

significantly longer time than the time required for the reflected shock wave to reach the top edge of the stamper. The high-pressure duration of the laser-induced shock wave was approximately three times longer than the laser exposure time, which was in the order of tens of nanoseconds [34,35]. Therefore, explosion-derived shock waves work well for imprinting thick plates.

This study has several limitations. Explosions typically release an explosive energy of several kJ/g. The long duration of the pressure, which is characteristic of the explosive-derived shock waves, is attributed to this energy. Excess energy was consumed in this study. In this method, the deformation of the polymer stamper must be maintained within an elastic range. Pressure and duration are critical to the

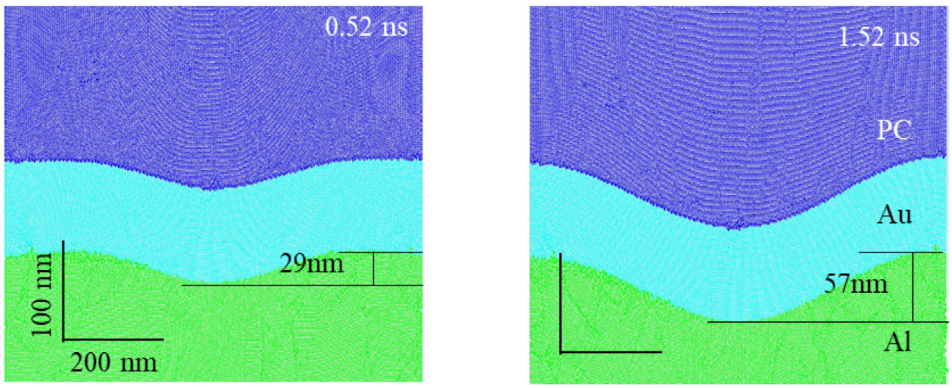

Fig. 6 – Imprinting process under high-pressure conditions ($H = 10$ mm). (a) Decrease of sinusoidal wave height at the most compressed timing. (b) Restoration of sinusoidal wave height by the PC restoring force.

accuracy of an imprint. While using explosives, the pressure value can be controlled by regulating the distance H, and the duration of action can be controlled by regulating the amount of explosives. Stamper geometries with sharp edges or high-aspect ratio geometries can cause plastic deformation or changes in the polymer state. The optimization of the energy and stamper geometry can be studied in the future.

4. Conclusion

Previous shock-imprinting technologies have been limited to thin metal foils as processing targets. To overcome this limitation, experiments related to shock imprinting on an Al plate using a polymer stamper were conducted. Furthermore, numerical simulations were performed to clarify the deformation mechanism between the polymer stamper and metal workpiece, leading to the following conclusions.

1. The underwater detonation of explosives produced a high-impulse shock wave. The shock wave compressed the thick polymer stamper onto the thick Al plate. Consequently, an imprint of approximately 69% of the sinusoidal wave height of the stamper was achieved on a 30×30 mm^2 area of the Al plate surface.
2. The shock wave compression temporarily reduced the height of the sine wave of the stamper. When the reflected shock wave generated at the stamper/workpiece boundary reached the stamper-free surface, the internal pressure on the PC surface decreased locally. The pressure drop established a restoring trend in the specific volume of the convexity (restoration of the sinusoidal wave height). The high-impulse shock wave continuously compressed the stamper, and the shape restoration of the stamper during this process contributed to the high imprinting accuracy.

5. Outlook

The results of this study have several possible applications. Metasurfaces are functional surfaces that convert electromagnetic wave properties into sub-wavelength structures. Sky radiators are functional surfaces that control the absorption and emission of infrared radiation to achieve radiative cooling using micrometer-order surface structures. A possible application of this technology is the creation of ultralarge sky radiators. This technology imprints microstructures on thick Al plates. The high thermal conductivity of Al and high heat capacity of the plate material lead to increased heat absorption from the structure, which is converted by the metasurface to thermal wavelengths that are not absorbed by the atmosphere. Currently, the implementation of metamaterials has only been envisioned for small electronic devices. This technology paves the way for outdoor applications of metamaterials.

Funding sources

This research received no specific grant from public, commercial, or not-for-profit funding agencies.

Data availability

None.

Declaration of competing interest

The authors declare that they have no known competing financial interests or personal relationships that could have appeared to influence the work reported in this paper.

Acknowledgments

none.

REFERENCES

[1] Gao H, Hu Y, Xuan Y, Li J, Yang Y, Martinez vRV, et al. Nanolithography. Large-scale nanoshaping of ultrasmooth

3D crystalline metallic structures. Science 2014;346:1352–6. https://doi.org/10.1126/science.1260139.
[2] Hu Y, Kumar P, Xu R, Zhao K, Cheng GJ. Ultrafast direct fabrication of flexible substrate-supported designer plasmonic nanoarrays. Nanoscale 2016;8:172–82. https://doi.org/10.1039/c5nr06899a.
[3] Chou SY. Nanoimprint lithography. J Vac Sci Technol B 1996;14:4129. https://doi.org/10.1116/1.588605.
[4] Vieu C, Carcenac F, Pépin A, Chen Y, Mejias M, Lebib A, et al. Electron beam lithography: resolution limits and applications. Appl Surf Sci 2000;164:111–7. https://doi.org/10.1016/S0169-4332(00)00352-4.
[5] Keller S, Chupakhin S, Staron P, Maawad E, Kashaev N, Klusemann B. Experimental and numerical investigation of residual stresses in laser shock peened AA2198. J Mater Process Technol 2018;255:294–307. https://doi.org/10.1016/j.jmatprotec.2017.11.023.
[6] Ye C, Liao Y, Cheng GJ. Warm laser shock peening driven nanostructures and their effects on fatigue performance in aluminum Alloy 6160. Adv Eng Mater 2010;12. https://doi.org/10.1002/adem.200900290. NA–.
[7] Cheng GJ, Pirzada D, Ming Z. Microstructure and mechanical property characterizations of metal foil after microscale laser dynamic forming. J Appl Phys 2007;101. https://doi.org/10.1063/1.2710334.
[8] Shen Z, Liu H, Wang X, Wang C. Surface degradation of micro-mold in micro-scale laser dynamic forming and its effects on workpiece. Opt Laser Technol 2019;117:114–25. https://doi.org/10.1016/j.optlastec.2019.03.047.
[9] Man J, Zhao J, Yang H, Song L, Liu D. Study on laser shock imprinting nanoscale line textures on metallic foil and its application in nanotribology. Mater Des 2020;193:108822. https://doi.org/10.1016/j.matdes.2020.108822.
[10] Liu Q, Hu X, Su C, Zhang C. Abrasion resistance of femtosecond pulsed laser processed micro molds of laser shock imprinting. Surf Coat Technol 2022;447. https://doi.org/10.1016/j.surfcoat.2022.128879.
[11] Lee JB, Choi KH, Yoo K. Innovative SU-8 lithography techniques and their applications. Micromachines 2015;6:1–18. https://doi.org/10.3390/mi6010001.
[12] Goswami D, Munera JC, Pal A, Sadri B, Scarpetti CLPG, Martinez vRV. Roll-to-roll nanoforming of metals using laser-induced superplasticity. Nano Lett 2018;18:3616–22. https://doi.org/10.1021/acs.nanolett.8b00714.
[13] Jin S, Wang Y, Motlag M, Gao S, Xu J, Nian Q, et al. Large-area direct laser-shock imprinting of a 3D biomimic hierarchical metal surface for triboelectric nanogenerators. Adv Mater 2018;30:1705840. https://doi.org/10.1002/adma.201705840.
[14] Jin S, Zhou Z, Sakr ESA, Motlag M, Huang X, Tong L, et al. Scalable nanoshaping of hierarchical metallic patterns with multiplex laser shock imprinting using soft optical disks. Small 2019;15:e1900481. https://doi.org/10.1002/smll.201900481.
[15] Tanaka S, Hasegawa K, Bataev I, Kubota A, Hokamoto K. Sub-micrometer and nanoscale imprinting on large-area foils using high-pressure underwater shock waves. Mater Des 2021;198:109341. https://doi.org/10.1016/j.matdes.2020.109341.
[16] Tanaka S, Inao D, Bataev I, Kubota A, Hokamoto K. Ultralarge-area shock imprinting using underwater shock wave and natural leaf mold. Manuf Lett 2021;27:8–12. https://doi.org/10.1016/j.mfglet.2020.11.004.
[17] Hasegawa K, Tanaka S, Bataev I, Inao D, Nishi M, Kubota A, et al. One-dimensional nanoimprinting using linear explosives. Mater Des 2021;203. https://doi.org/10.1016/j.matdes.2021.109607.
[18] Xiong F, Yang H, Liu K, Man J, Chen H. Effect of imprinting times and stress annealing on warm laser shock imprinting. Microsyst Technol 2020;26:353–66. https://doi.org/10.1007/s00542-019-04552-7.
[19] Haifeng Y, Fei X, Kun L, Jiaxiang M, Haoxue C, Hao L, et al. Research on temperature-assisted laser shock imprinting and forming stability. Opt Laser Eng 2019;114:95–103. https://doi.org/10.1016/j.optlaseng.2018.11.002.
[20] Yang H, Liu K, Liu H. Microscale laser shock imprinting of micro-molds with different sizes and shapes. Opt Appl 2018;48:671–86. https://doi.org/10.5277/oa180412.
[21] Shen Z, Zhang L, Li P, Liu H, Liu K, Lin Y, et al. Altering the surface wettability of copper sheet using overlapping laser shock imprinting. Appl Surf Sci 2021;543. https://doi.org/10.1016/j.apsusc.2020.148736.
[22] Hasegawa K, Tanaka S, Bataev I, Inao D, Nishi M, Kubota A, et al. Toward a better understanding of shock imprinting with polymer molds using a combination of numerical analysis and experimental research. Materials 2022;15. https://doi.org/10.3390/ma15051727.
[23] Meyers MA. Dynamic behavior of materials. A Wiley-Interscience Publication; 1994.
[24] Fu S, Wang Y, Wang Y. Tension testing of polycarbonate at high strain rates. Polym Test 2009;28:724–9. https://doi.org/10.1016/j.polymertesting.2009.06.002.
[25] Su W, Luo Y, Ding Y, Wu J. Low-cost surface plasmon resonance refractive index sensor based on the metal grating in DVD-ROM disc. Sens Actuators, A 2021;330. https://doi.org/10.1016/j.sna.2021.112858.
[26] Corbett BM. Numerical simulations of target hole diameters for hypervelocity impacts into elevated and room temperature bumpers. Int J Impact Eng 2006;33:431–40. https://doi.org/10.1016/j.ijimpeng.2006.09.086.
[27] Welly SM, Field JE. Strain rate sensitivity of polymers in compression from low to high rates. DYMAT. journal. 1994:211–27.
[28] Marsh S. LASL shock Hugoniot data. Berkeley a.o: University of California Press; 1980.
[29] Johnson GR, Cook WH. Fracture characteristics of three metals subjected to various strains, strain rates, temperatures and pressures. Eng Fract Mech 1985;21:31–48. https://doi.org/10.1016/0013-7944(85)90052-9.
[30] Senthil K, Iqbal MA. Effect of projectile diameter on ballistic resistance and failure mechanism of single and layered aluminum plates. Theor Appl Fract Mech 2013;67–68:53–64. https://doi.org/10.1016/j.tafmec.2013.12.010.
[31] Pierazzo E, Artemieva N, Asphaug E, Baldwin EC, Cazamias J, Coker R, et al. Validation of numerical codes for impact and explosion cratering: impacts on strengthless and metal targets. Meteorit Planet Sci 2008;43:1917–38. https://doi.org/10.1111/j.1945-5100.2008.tb00653.x.
[32] Tanaka S, Bataev I, Nishi M, Balagansky I, Hokamoto K. Micropunching large-area metal sheets using underwater shock wave: experimental study and numerical simulation. Int J Mach Tool Manufact 2019;147. https://doi.org/10.1016/j.ijmachtools.2019.103457.
[33] Murata K, Kato Y. Application of PVDF pressure gauge for pressure measurements of non-ideal explosives. Int J Soc Mater Eng Resour 2010;17:112–4. https://doi.org/10.5188/ijsmer.17.112.
[34] Liu H, Lu M, Wang X, Shen Z, Gu C, Gu Y. Micro-punching of aluminum foil by laser dynamic flexible punching process. Int J Material Form 2015;8:183–96. https://doi.org/10.1007/s12289-013-1159-2.
[35] Fabbro R, Fournier J, Ballard P, Devaux D, Virmont J. Physical study of laser-produced plasma in confined geometry. J Appl Phys 1990;68:775–84. https://doi.org/10.1063/1.346783.